Research Article Vol. 32, No. 26 / 16 Dec 2024 / Optics Express 47549
Optics EXPRESS

Optimization of crystal length in a pulse-pumped up-conversion single-photon detector for decoding femtosecond time-bin qubits

YUTA KOCHI,[1,2] SUNAO KURIMURA,[3] AND JUNKO ISHI-HAYASE[1,2,*]

[1]School of Fundamental Science and Technology, Keio University, Kanagawa 223-8522, Japan
[2]Center for Spintronics Research Network, Keio University, Kanagawa 223-8522, Japan
[3]National Institute for Materials Science, Ibaraki 305-0047, Japan
[*]hayase@appi.keio.ac.jp

Abstract: In advancing ultrafast quantum communication and computing, it is crucial to develop precise time-resolved measurement techniques for single-photon pulses. However, the measurement of photonic qubits, especially time-bin qubits, is limited by the temporal resolution of single-photon detectors, typically around tens of picoseconds. In this study, we developed a pulse-pumped up-conversion single-photon detector (UCSPD) using periodically poled Mg-doped stoichiometric lithium tantalate (PPMg: SLT) crystals of varying lengths to optimize femtosecond up-conversion. We evaluated the UCSPD's efficiency and temporal resolution using a convolution model that accounts for group delay in nonlinear crystals. Our results demonstrate that the model calculations enable the accurate prediction of the crystal length dependence of temporal resolution and up-conversion efficiency without fitting parameters. The UCSPD achieved 415 fs resolution and 10.1 % efficiency with a 2 mm crystal, enabling successful characterization of time-bin qubits with 800 fs pulse intervals.

© 2024 Optica Publishing Group under the terms of the Optica Open Access Publishing Agreement

1. Introduction

In recent years, the development of quantum communication and quantum computing technologies utilizing photons has garnered significant attention. A key component of these technologies is the ability to accurately measure single-photon pulses with high temporal resolution. However, temporal resolution of conventional single-photon detectors is typically limited to 10~100 ps range. Recently, Korzh *et al.* [1] achieved a breakthrough with superconducting nanowire single-photon detectors, demonstrating a sub-3 picosecond temporal resolution. Nevertheless, achieving ~100 fs temporal resolution with single-photon detectors remains a challenge while femtosecond single-photon pulses have already been generated [2]. Consequently, the temporal spacing of photonic qubits, particularly time-bin qubits used in prior quantum communication demonstrations, has been constrained to the sub-nanosecond range [3–6]. Focusing on relative phase evaluation, Donohue *et al.* [7] demonstrated the determination of time-bin qubit phases with a pulse interval (Δt) of 2.2 ps. They decoded phase information from variations in frequency components, however, the measurement accuracy was constrained by the monochromator's resolution, which currently limited the pulse interval to approximately $\Delta t \sim 1$ ps. Several demonstrations of time-bin qubit decoding with picosecond-scale time intervals have been achieved using an optical Kerr effect or by employing separate pulses with different polarizations [8–11]. However, due to the need to eventually detect the qubits with single-photon detectors, the time intervals were typically stretched to the nanosecond range before decoding. This not only complicates the experimental setup but also prevents full utilization of the advantages offered by ultrafast communications.

#542524 https://doi.org/10.1364/OE.542524
Journal © 2024 Received 25 Sep 2024; revised 25 Nov 2024; accepted 29 Nov 2024; published 13 Dec 2024

Optics EXPRESS

To enhance temporal resolution, time-gating methods that have utilized nonlinear effects with ultrashort pulses have been developed. One such method was the optical Kerr gate, which has demonstrated measurements of single-photon pulse with a temporal resolution of 224 fs [12]. However, this technique relies on a third-order nonlinear optical effect, making it challenging to increase detection efficiency [13,14]. Another promising method is the frequency up-conversion single-photon detector (UCSPD). This detector has been designed to detect photons at telecom wavelengths using Si APDs, which offer higher efficiency compared to InGaAs APDs [15,16]. Recent implementations of UCSPDs using continuous-wave (CW) lasers as pump light have achieved up-conversion efficiencies exceeding 90 % [17–19]. In these systems, both the temporal resolution and dead time is influenced by the performance of the Si APDs. On the other hand, employing a femtosecond pulse laser as the pump light has enabled femtosecond order temporal resolution [20–24]. Kuzucu *et al.* [25,26] measured a temporal waveform correlation of photon pairs using a UCSPD with a 1-mm-long periodically poled Mg-doped stoichiometric lithium tantalate (PPMg:SLT) crystal and a femtosecond pulse laser. In sum-frequency generation within the femtosecond regime, the process is significantly affected by group delay in the crystal, making it challenging to increase up-conversion efficiency by simply extending the crystal length, as is possible with CW pumping. In fact, using a longer crystal can degrade temporal resolution and saturate the up-conversion efficiency due to the group delay. To date, however, no quantitative evaluation of the efficiency or temporal resolution, nor an estimation of the optimal crystal length, has been conducted for pulse-pumped UCSPDs operating in the femtosecond regime. Recently, Allgaier *et al.* [27,28] achieved high temporal resolution and up-conversion efficiency by employing a 27-mm-long periodically poled lithium niobate (PPLN) crystal in a waveguide that satisfied group velocity matching (GVM) between the pump and signal beams. However, this crystal features a unique 4.4 μm periodically poled period, making it extremely difficult to obtain. In any case, there are no demonstrations on measuring femtosecond time-bin qubits with pulse intervals shorter than 1 ps.

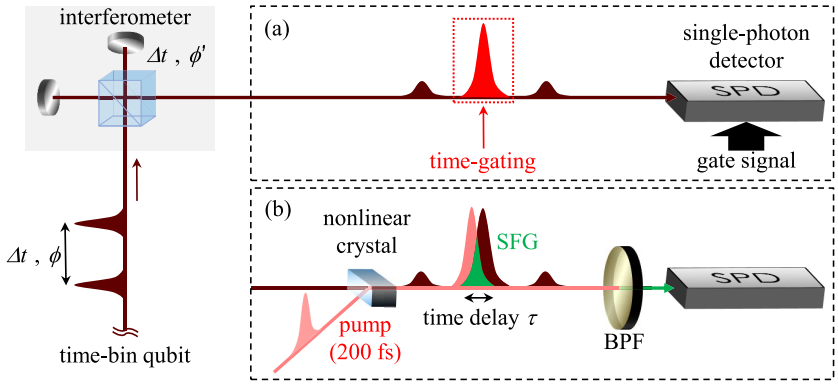

Fig. 1. (a) Previous method for evaluating time-bin qubits and (b) the current method employing frequency up-conversion techniques. SFG: sum-frequency generation; BPF: bandpass filter.

In this study, a UCSPD specifically developed for measuring femtosecond range ultrashort pulse signals was employed (see Fig. 1(b)). To evaluate the temporal resolution and up-conversion efficiency of this detector, commercial PPMg:SLT crystals of varying lengths were utilized. By fine-tuning the crystal length and pump power, the efficiency and temporal resolution of the UCSPD were quantitatively assessed. Additionally, a convolution model was introduced to quantitatively evaluate the dependence of the detector's performance on crystal length. Our results show that this model accurately predicts the crystal length dependence of sum-frequency

Optics EXPRESS

waveforms using only constants, such as group delay and pulse width, without any fitting parameters. This model enabled us to estimate the optimal crystal length for femtosecond UCSPD across arbitrary wavelengths and pulse widths using only the group delay of nonlinear crystals. As a result, the optimized UCSPD successfully evaluated the relative phase of pseudo femtosecond time-bin qubits with the shortest pulse interval reported thus far, Δt = 800 fs.

2. Performance of UCSPD

2.1. Experimental setup

The UCSPD was developed to overcome the performance limitations inherent in conventional single-photon detectors. This device employs a frequency up-conversion technique, where signal photons are converted into visible photons through sum-frequency generation (SFG) upon introduction into the detector. Utilizing a femtosecond pulse laser as the pump light, SFG occurs exclusively when there is temporal overlap between the signal photons and the pump pulse. By detecting the frequency component of SFG using commercial single-photon detectors, such as Si APDs, femtosecond order temporal resolution is achieved through time-gating of the signal waveforms.

Figure 2 illustrates the schematic setup of the UCSPD. An 820 nm femtosecond Ti:Sapphire laser (Coherent Mira-XP, pulse width Δ_p: 200 fs, repetition frequency: 76.3 MHz) was utilized to pump the nonlinear crystals, paired with a 1520 nm pulse from an optical parametric oscillator (Coherent Mira OPO-X, pulse width Δ_s: 240 fs) serving as the signal light. For frequency up-conversion, 1 mol.% MgO-doped stoichiometric lithium tantalate (PPMg:SLT) bulk crystals were employed. These crystals offer considerable benefits, including low absorption and dispersion coupled with high nonlinearity of 10 pm/V [29]. Their minimal linear and nonlinear absorbances [30] contribute to thermally stable operation even under high-power green light [31]. Notably, due to its short-band edge below 280 nm [32], the refractive index dispersion of PPMg:SLT in the long-wavelength range is substantially lower than that of lithium niobate (LN) and potassium titanyl phosphate (KTP). This characteristic effectively minimizes pulse broadening and reduces group velocity mismatch [25] between signal and pump pulses. PPMg:SLT crystals of 1, 2, and 3 mm lengths with periodically poled periods of 8.55 μm were selected, optimal for type-0 phase-matched SFG (820 nm + 1520 nm $\rightarrow$ 533 nm) at a crystal temperature of 85°C. The wavelength that satisfies the phase matching condition can be adjusted through the temperature control of the crystal. When the pump wavelength is fixed at 820 nm, the signal wavelength satisfies the phase matching condition within the range of approximately 1510 to 1560 nm by varying the temperature from 20 to 200°C. The pump and signal pulses were focused through separate lenses to prevent chromatic-aberration-induced focal shifts [33]. The focal length of the pump beam lens f_p was 200 mm, and that of the signal beam lens f_s was 150 mm. The beam spot sizes were set to 80 μm for the signal and 100 μm for the pump. The beam diameters were set larger than the optimal values estimated based on the crystal length, according to Boyd *et al.*'s theory [34] since focusing to a smaller spot size could introduce instability due to optical path fluctuations and unexpected noise, such as supercontinuum generation. Moreover, by using this looser focus, we were able to effectively compare the crystal length dependence of the UCSPD performance independently of other factors. The up-converted photons were subsequently detected using a Si APD (Hamamatsu C13001-01). The quantum efficiency of used Si APD was 41 % at 532 nm, and the dark count rate was 100 cps.

2.2. Results and discussion

The initial assessment of temporal resolution and up-conversion efficiency was performed by measuring a single pulse at the single-photon level (average photon number: 0.1/pulse) using the UCSPD, with the pump power set to 300 mW. The lengths of the PPMg:SLT crystals were

Optics EXPRESS

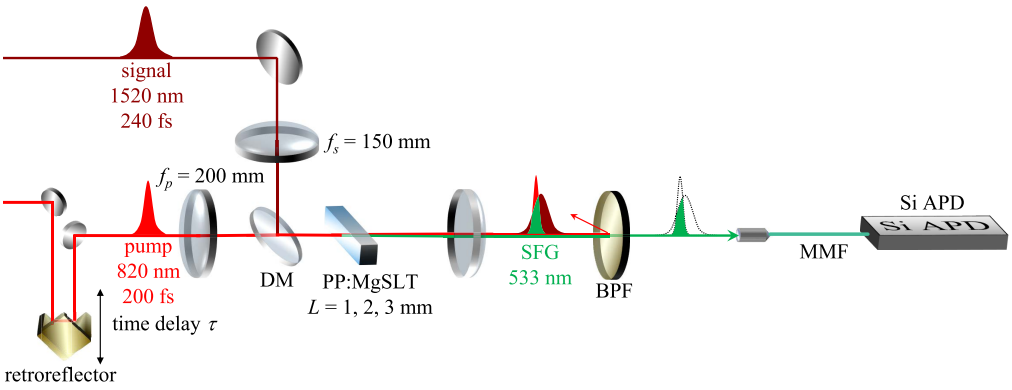

Fig. 2. Schematic of the UCSPD system. BPF: band-pass filter; DM: dichroic mirror; MMF: multimode fiber; Si APD: silicon avalanche photodiode.

varied, and the positions of the lenses were readjusted to optimize the focal points of the pump and signal light, thereby maximizing the up-conversion efficiency. Figure 3(a) shows the count rate of the up-converted photons as a function of the time delay between the signal and pump pulses. It was observed that the peak count rate increased with the crystal length from 1 to 2 mm but reached saturation with a 3 mm crystal due to the reduced temporal overlap between the pump and signal pulses, which was caused by group delay in the crystal.

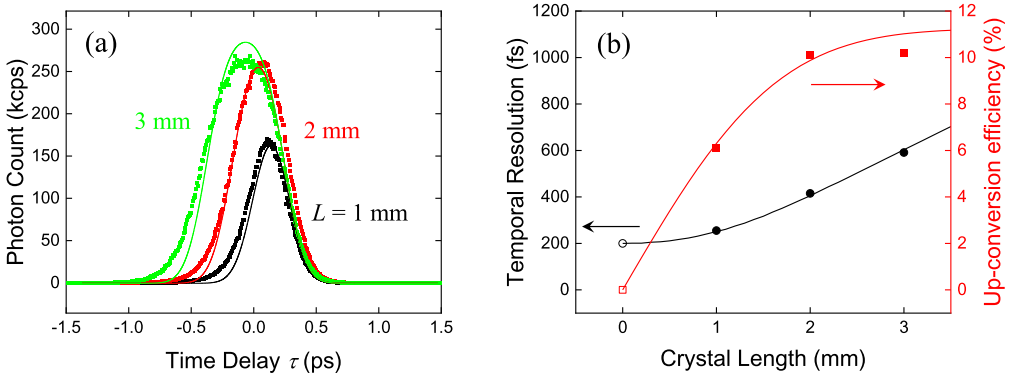

Fig. 3. (a) Measured waveforms of single-photon level pulses obtained with the UCSPD are shown. Solid lines represent the calculated waveforms using our convolution model. (b) Graph showing temporal resolution (black) and up-conversion efficiency (red) as functions of crystal length. Square dots represent experimental data, while solid lines are theoretical predictions based on Eq. (4). The hollow dots at a crystal length of 0 mm represent estimated values, with an up-conversion efficiency of 0 % and a temporal resolution of 200 fs (same as the pump pulse width).

To estimate the temporal resolution, the temporal resolution function $T(t)$ is defined as follows:

$$T(t) \equiv (P * G)(t)$$
$$G(t) = \begin{cases} 1 & -\frac{\tau_g L}{2} \le t \le \frac{\tau_g L}{2} \\ 0 & t < -\frac{\tau_g L}{2},\ \frac{\tau_g L}{2} < t, \end{cases} \quad (1)$$

where $P(t)$ represents the temporal waveform of the pump pulse, and $G(t)$ is a rectangular function with a width equal to the group delay $\tau_g L$ (with τ_g being 204.3 fs/mm [35]) between the pump

Optics EXPRESS

and signal pulses. This model assumes that the pump electric field is sufficiently weak, such that the SFG intensity is proportional to the pump power. The waveforms measured by the UCSPD, $S_{\text{out}}(t)$, can be expressed as:

$$S_{\text{out}}(t) = (S_{\text{in}} * T)(t). \tag{2}$$

Assuming Gaussian temporal waveforms for both the pump and signal pulses,

$$\begin{aligned} P(t) &\propto \exp\left[-\left(\frac{2\sqrt{\ln 2}}{\Delta_{\text{p}}}t\right)^2\right] \\ S_{\text{in}}(t) &\propto \exp\left[-\left(\frac{2\sqrt{\ln 2}}{\Delta_{\text{s}}}t\right)^2\right], \end{aligned} \tag{3}$$

waveform $S_{\text{out}}(t)$ is computed as follows:

$$\begin{aligned} S_{\text{out}}(t) &= (S_{\text{in}} * T)(t) \\ &\propto \int_{-\tau_{\text{g}}L/2}^{\tau_{\text{g}}L/2} \exp\left[-\frac{4\ln 2}{\Delta_{\text{p}}^2+\Delta_{\text{s}}^2}(t-\tau)^2\right] d\tau \\ &= \int_{-\tau_{\text{g}}L/2-t}^{\tau_{\text{g}}L/2-t} \exp\left[-\frac{4\ln 2}{\Delta_{\text{p}}^2+\Delta_{\text{s}}^2}\tau'^2\right] d\tau' \\ &\propto \text{erf}\left[\sqrt{\frac{\ln 2}{\Delta_{\text{p}}^2+\Delta_{\text{s}}^2}}\left(\tau_{\text{g}}L-2t\right)\right] - \text{erf}\left[\sqrt{\frac{\ln 2}{\Delta_{\text{p}}^2+\Delta_{\text{s}}^2}}\left(-\tau_{\text{g}}L-2t\right)\right]. \end{aligned} \tag{4}$$

This convolution model illustrates that as the crystal length (L) increases, the corresponding group delay ($\tau_{\text{g}}L$) also increases, causing the measured waveform $S_{\text{out}}(t)$ to approximate a rectangular shape. Temporal resolution was defined as the FWHM of $T(t)$. Analyzing the data presented in Fig. 3(a), the temporal resolutions of the UCSPD were estimated to be 255, 415, and 591 fs for crystal lengths of 1, 2, and 3 mm, respectively, as indicated by the square dots in Fig. 3(b). The pulse shapes of solid lines in Fig. 3(a) show good agreement with the experimental results across all crystal lengths, despite the calculation using Eq. (4) involving only the group delay value of 204.3 fs/mm and the pulse widths of pump and signal pulses. To compare the experimental and calculated waveforms, we only adjusted the amplitude of the calculated waveforms for the 1-mm-long crystal. Although the relative amplitudes between the 1, 2, and 3 mm crystals were kept unchanged, the calculated waveforms closely replicates the experimental results. In this model, it was assumed that there were no changes in the beam diameters of the signal or pump, nor any pulse broadening (chirping) due to group velocity dispersion. This approximation is valid because, in femtosecond range UCSPD, increasing the crystal length reduces pulse overlap due to group delay, and only millimeter-scale crystals can be practically used. Consequently, changes in beam diameter have a negligible effect, and the calculated results closely match experimental values, validating this assumption. However, when the crystal length reaches around 3 mm, changes in beam diameter can no longer be ignored. In the experiments, the spot size of the signal beam was set smaller than that of the pump beam to ensure full overlap. Nonetheless, due to the shorter wavelength of the pump light, it was observed that for crystal lengths exceeding 2 mm, the signal beam diameter becomes partially larger than the pump beam, reducing spatial overlap. In practice, for the 3-mm-long crystal, the calculated waveform displayed a larger amplitude than observed experimentally.

Figure 3(b) depicts the dependence of the temporal resolution and up-conversion efficiency on crystal length. These results demonstrate that the model outlined in Eq. (4) adequately explains the

Optics EXPRESS

experimental results using only constants such as the group delay of the crystals and pulse widths, with no additional fittings required. This suggests that it will enable the selection of the appropriate crystal length according to the required temporal resolution and up-conversion efficiency for each experiment in the future femtosecond UCSPD designs. Regarding up-conversion efficiency, the calculated value for the 3-mm-long crystal exceeds the experimental result due to variations in beam diameter. Therefore, further analysis is needed for longer crystal lengths, and future research should focus on calculations that account for changes in beam diameter.

The subsequent investigation focused on the dependence of up-conversion efficiency (η_{UC}) and the detection limit of the UCSPD on pump power. As shown in Fig. 4(a), the up-conversion efficiency increases proportionally with the pump power of up to 400 mW and the efficiency begun to saturate beyond this power. In our experiments, including those conducted thereafter, we used a pump power of 300 mW, and it was found that our simple model is sufficiently applicable at this intensity. For higher pump powers, such as in SFG under high-intensity pumping, it will be necessary to consider the effects of reverse processes and the saturation of conversion efficiency. Concurrently, Fig. 4(b) illustrates that the noise count rate rises exponentially with increasing up-conversion efficiency. Considering that the dark count rate of the Si APD was approximately 100 cps, this noise is primarily attributable to photons originating from the PPMg:SLT crystals. The predominant source of noise photons is the spontaneous parametric down-conversion (SPDC) process, which is reconverted by the pump light, as Raman scattering is minimal in crystals of a few millimeters in length [36]. Previous studies have suggested that SPDC noise can be reduced by employing a longer pump wavelength of approximately 1.9 μm [37–39].

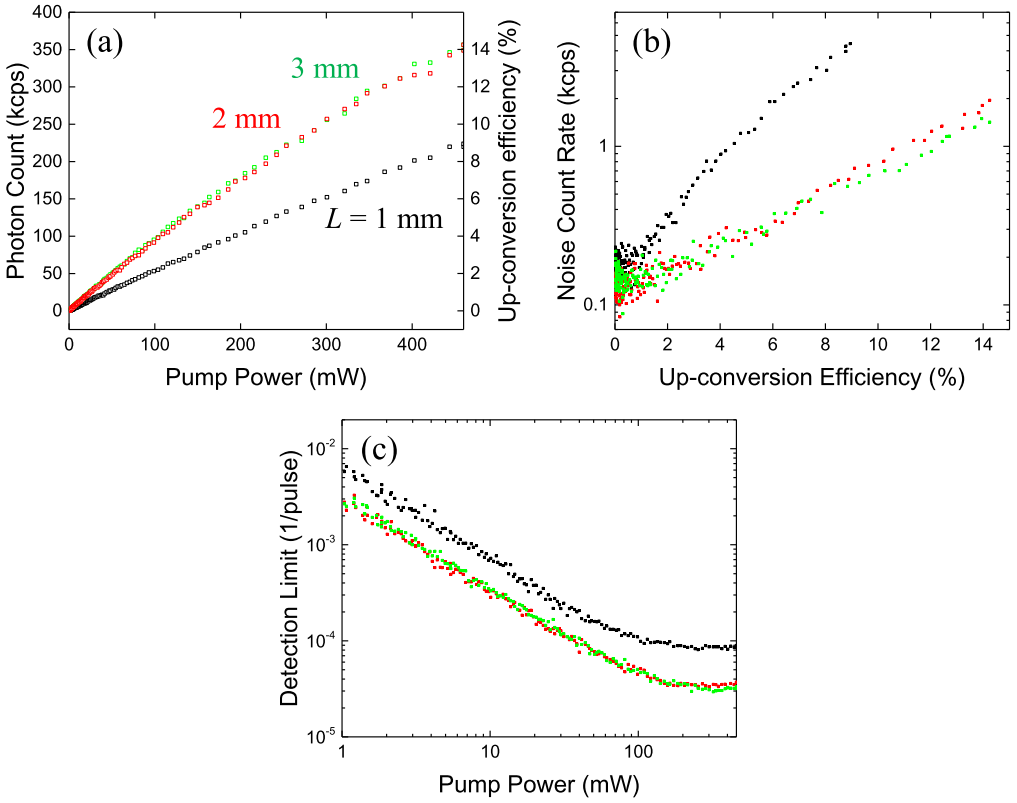

Fig. 4. (a) Up-conversion efficiency plotted against pump power for different crystal lengths: black for 1 mm, red for 2 mm, green for 3 mm. (b) Variation in noise count rates. (c) Average number of photons per pulse at the detection threshold.

Optics EXPRESS

The detection limit is defined as the number of photons resulting in a count rate three times the standard deviation of the noise count rate (σ_{NCR}):

$$\text{Average photon number of the detection limit} = \frac{3\sigma_{\mathrm{NCR}}}{\eta_{\mathrm{tot}}}. \tag{5}$$

Here, $\eta_{\mathrm{tot}} = \eta_{\mathrm{UC}} \times \eta_{\mathrm{other}}$ represents the total UCSPD system efficiency, which includes the efficiency η_{other} considering other losses such as the Si APD detection efficiency of 41 %, fiber coupling efficiency of 85 %, and filter transmittance of 94 %. Fig. 4(c) illustrates that the detection limit remains relatively stable for pump powers exceeding 200 mW, registering minimum values of 8.6, 3.3, and 3.1 $\times 10^{-5}$ photons per pulse for crystal lengths of 1, 2, and 3 mm, respectively, at a pump power of 300 mW. The internal up-conversion efficiencies η_{UC} were calculated to be 6.1, 10.1, and 10.2 % for the 1, 2, and 3 mm crystals, respectively (Table 1). In this experiment, we did not optimize the beam diameter for the above-mentioned reasons. However, if the beam diameter can be optimized for each crystal length, further efficiency improvements expected to be possible. Furthermore, we did not use a transform-limited pulse for the pump light of the UCSPD. Compared to a laser with the same pulse width, a transform-limited pulse has a narrower spectrum, which increases the frequency components of the pump light within the crystal's bandwidth, and is expected to result in higher conversion efficiency. When compared to other detectors, the UCSPD achieves notably lower noise levels than InGaAs detectors at room temperature (300 K) and delivers high temporal resolution on the femtosecond scale (Table 2).

Table 1. Dependence of UCSPD performance on crystal length.

Crystal Length	Temporal Resolution	Up-conversion Efficiency	Noise Count Rate
1 mm	255 fs	6.1 %	1910 cps
2 mm	415 fs	10.1 %	800 cps
3 mm	591 fs	10.2 %	700 cps

Table 2. Performance comparison of various single-photon detectors at telecom wavelength. Typical values for the SNSPD are based on SCONTEL TCOPRS-CCR-TW-60.

Single-photon Detector	Operating Temperature	Temporal Resolution	Quantum Efficiency	Noise Count Rate	Dead Time
InGaAs/InP [16]	223 K	170 ps	27.5 %	1200 cps	100 ns
SNSPD (Typ.)	2.1 K	57 ps	80 %	10 cps	10 ns
SNSPD [1]	0.9 K	4.3 ps	-	-	-
optical Kerr gate [12]	300 K	0.2 ps	-	-	-
UCSPD (CW) [19]	300 K	400 ps	40.2 %	200 cps	100 ns
UCSPD (pulse) [27,28]	300 K	0.3 ps	16.9 %	-	-
UCSPD (this work)	300 K	0.4 ps	3.3 %	700 cps	-

Recent studies have shown that GVM can be effectively mitigated using type-II quasi-phase matching in PPLN crystals across the wavelength range of 780–1560 nm [40,41]. Allgaier's research [27,28] reached high up-conversion efficiency and temporal resolution by addressing this phase matching in a PPLN crystal with a periodically poled period of 4.4 μm within a 27 mm optical waveguide. Although effective, this setup presents significant challenges, particularly because obtaining the crystal required for this design is extremely difficult. In contrast, our UCSPD achieves femtosecond order temporal resolution and practical detection efficiency using commercially available crystals, offering a more accessible and equally robust

Optics EXPRESS

alternative. Moreover, our simple convolution model accurately represented the experimental results using only the group delay value and the pulse widths of the pump and signal pulses. This model provides the optimal crystal length for femtosecond regime up-conversion across various nonlinear crystals, wavelengths, and pulse widths.

3. Evaluation of femtosecond time-bin qubits

3.1. Experimental setup

Figure 5 depicts the experimental setup utilized for generating and assessing pseudo femtosecond time-bin qubits. This arrangement comprises two unbalanced Michelson interferometers, each configured with identical time delays (Δt), which establish the pulse intervals for the time-bin qubits. Each interferometer is equipped with a polarization beam splitter and two quarter-wave plates to minimize light loss upon reflection. Additionally, a cover glass was positioned in one arm of each interferometer to facilitate the adjustment of the relative phase by varying the angle of the glass plate.

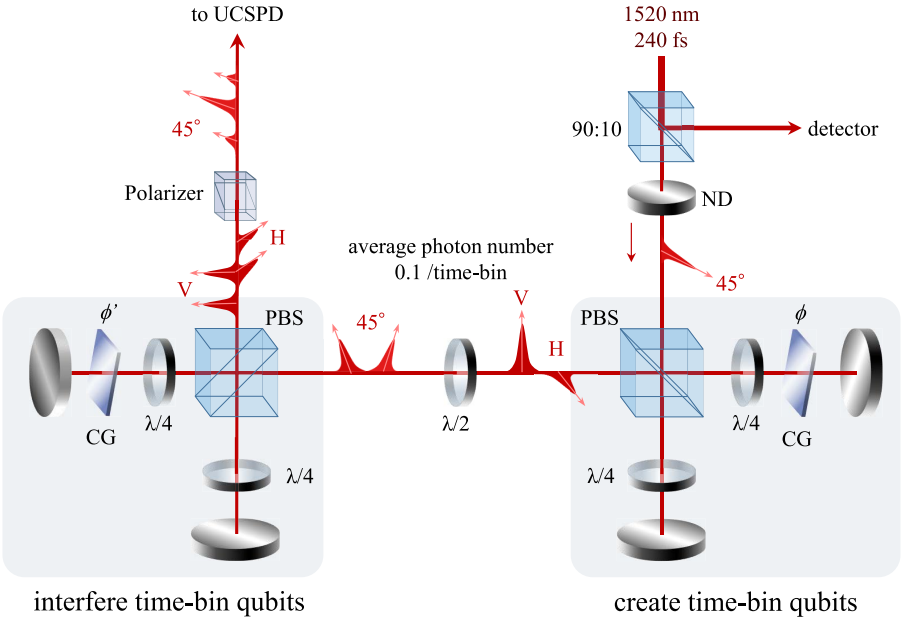

Fig. 5. Experimental setup for generating and evaluating femtosecond time-bin qubits. CG: cover glass; ND: neutral density filter; PBS: polarization beam splitter; $\lambda/2$: half-wave plate; $\lambda/4$: quarter-wave plate.

For this experiment, light pulses at the single-photon level (average photon number: 0.1/pulse) from an optical parametric oscillator were employed as the light source. The time delay Δt was set to 800 fs, significantly exceeding both the pulse width and the temporal resolution of the UCSPD. As a single-photon traverses the interferometer, it is transformed into a time-bin qubit encoded as $\frac{1}{\sqrt{2}}(|e\rangle + e^{i\phi}|l\rangle)$, where $|e\rangle$ denotes the photon traveling through the short arm, and $|l\rangle$ signifies the photon passing through the long arm. As these time-bin qubits reenter the interferometer, each photon state evolves into $|e\rangle \rightarrow \frac{1}{\sqrt{2}}(|ee\rangle + e^{i\phi'}|el\rangle)$ and $|l\rangle \rightarrow \frac{1}{\sqrt{2}}(|el\rangle + e^{i\phi'}|ll\rangle)$, resulting in the output state $|\psi_{\text{out}}\rangle$ of the interferometer:

$$|\psi_{\text{out}}\rangle \propto |ee\rangle + (e^{i\phi} + e^{i\phi'})|el\rangle + |ll\rangle. \tag{6}$$

Optics EXPRESS

The ratios of the probability amplitudes P_{ee}, P_{el}, and P_{ll} (corresponding to photon states $|ee\rangle$, $|el\rangle$, and $|ll\rangle$, respectively) are analyzed to provide insights into the system dynamics:

$$P_{ee} : P_{el} : P_{ll} = 1 : 4\cos^2\left(\frac{\phi - \phi'}{2}\right) : 1. \tag{7}$$

Therefore, by time-gating the central peak P_{el} using the UCSPD, the relative phase difference $\phi - \phi'$ of the time-bin qubits can be evaluated effectively. We used a 2-mm-long PPMg:SLT crystal and 300 mW pump power for the UCSPD.

3.2. Results and discussion

Figure 6(a) shows the measured temporal waveforms of pseudo femtosecond time-bin qubits at various relative phases. It is evident that the waveforms of time-bin qubits with an interval of only 800 fs have been clearly measured using our UCSPD. The solid blue line represents the estimated original waveforms, reconstructed through deconvolution using the temporal resolution function $T(t)$. This demonstrates that our convolution model for the UCSPD enables accurate reconstruction of the original signal waveforms prior to measurement. Notably, the interference waveforms of time-bin qubits with pulse intervals as short as 800 fs are clearly observable when the pump pulse delay is set to 0 fs. Under these detection conditions, the detection limit of our UCSPD was 3.3×10^{-5}/time-bin, which is sufficient to measure single-photon pulses. This underscores the capability of our technique to achieve high precision in time-resolved measurement and reconstruction of waveforms in the femtosecond range. For measurements requiring even higher temporal resolution, a 1-mm-long crystal can be used. In this case, although the up-conversion efficiency decreases to 6.1% and the average photon number detection limit reduces to 8.6×10^{-5}/time-bin, this adjustment enables pulse intervals to be shortened to as close as 540 fs, thereby significantly enhancing the temporal resolution capabilities.

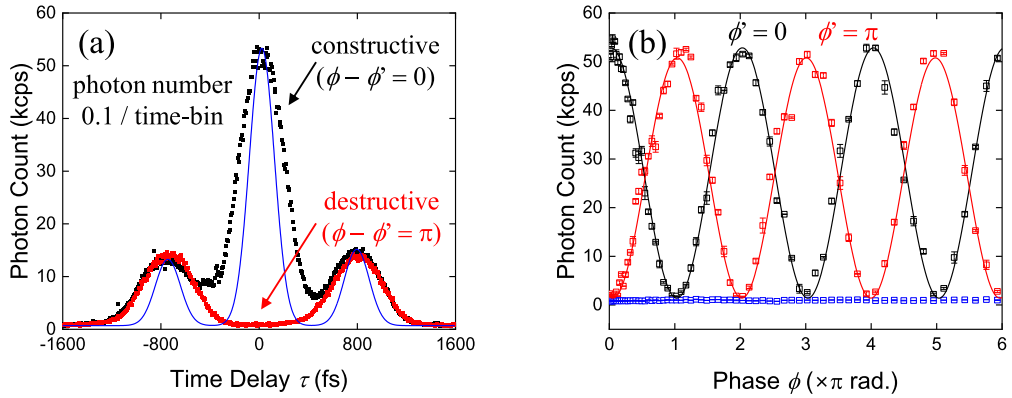

Fig. 6. (a) Temporal waveforms of time-bin qubits, with black and red dots representing experimental data and the solid blue line depicting the original waveforms reconstructed by deconvolution using the temporal resolution function $T(t)$. (b) Variation in the count of the central peak at $\tau = 0$ fs in (a), with solid lines representing sine curve fittings to the data. Black: $\phi' = 0$; Red: $\phi' = \pi$. Blue squares represent background noise

Subsequently, with the delay time maintained at 0 fs, the variation in interference intensity P_{el} as a function of the relative phase $\phi - \phi'$ was measured. Figure 6(b) illustrates how the count varies with the relative phase, demonstrating visibilities of $98.2 \pm 0.09\%$ for $\phi' = 0$ and $98.1 \pm 0.09\%$ for $\phi' = \pi$. Hence, we have successfully optimized and evaluated the performance of the femtosecond UCSPD, achieving high-visibility decoding of time-bin qubits with an 800 fs pulse interval, which was previously challenging to measure.

Optics EXPRESS

4. Conclusion

In this study, a pulse-pumped up-conversion single-photon detector (UCSPD) was developed using commercially available bulk PPMg:SLT crystals. To quantitatively assess the temporal resolution and up-conversion efficiency of the UCSPD, we introduced a convolution model to estimate the optimal crystal length. Using this model, we accurately simulated the crystal length dependence of the temporal resolution and up-conversion efficiency of the UCSPD using only the group delay value and the pulse widths of the pump and signal pulses. This suggests that it will enable the selection of the appropriate crystal length according to the required temporal resolution and efficiency for each experiment using various types of nonlinear crystals, wavelengths, and pulse widths in the future design of femtosecond UCSPD. In our UCSPD, we determined that the optimal crystal length for our setup was 2 mm. With this crystal length, the UCSPD demonstrated a temporal resolution of 415 fs, significantly surpassing conventional single-photon detectors, and achieved an up-conversion efficiency of 10.1%. Additionally, this study successfully evaluated single-photon-level femtosecond time-bin qubits with a pulse interval Δt of 800 fs, the shortest interval reported to date. This methodology promises a substantial enhancement in the information density of quantum communication—potentially increasing it by three orders of magnitude—and in accelerating communication speeds. Future work will focus on further exploring the characteristics of time resolution and output waveforms identified in this study. This includes optimizing beam diameter conditions and conducting detailed theoretical analyses using propagation equations for the frequency mixing of ultrashort pulses. Moreover, this method requires sweeping the stage to measure a wide range of waveforms. However, by integrating it with time-to-space conversion [42], time-to-frequency conversion [43], and the dual-comb-based Asynchronous Optical Sampling (ASOPS) technique [24] will enable rapid waveform acquisition over a wide time range without the need to move the stage. Subsequent research will also involve evaluating time-bin qubits with nonclassical light sources and exploring their potential for storage and retrieval in broadband quantum memory systems utilizing quantum dots [44,45], thereby advancing the field of quantum communication technology.

Funding. Japan Society for the Promotion of Science (Grant-in-Aid for JSPS Fellows No. JP23KJ1916); Core Research for Evolutional Science and Technology (JST CREST No. JPMJCR24A5).

Acknowledgments. This work was supported by Center for Spintronics Research Network and the Program for the Advancement of Next Generation Research Projects at Keio University. The authors extend their gratitude to Prof. R. Shimizu for insightful discussions and technical support.

Disclosures. The authors declare no conflict of interest.

Data availability. Data underlying the results presented in this paper are not publicly available at this time but may be obtained from the authors upon reasonable request.

References

1. B. Korzh, Q.-Y. Zhao, J. P. Allmaras, *et al.*, "Demonstration of sub-3 ps temporal resolution with a superconducting nanowire single-photon detector," Nat. Photonics **14**(4), 250–255 (2020).
2. E. Y. Zhu, Z. Tang, L. Qian, *et al.*, "Poled-fiber source of broadband polarization-entangled photon pairs," Opt. Lett. **38**(21), 4397–4400 (2013).
3. A. Martin, F. Kaiser, A. Vernier, *et al.*, "Cross time-bin photonic entanglement for quantum key distribution," Phys. Rev. A **87**(2), 020301 (2013).
4. E. Saglamyurek, J. Jin, V. B. Verma, *et al.*, "Quantum storage of entangled telecom-wavelength photons in an erbium-doped optical fibre," Nat. Photonics **9**(2), 83–87 (2015).
5. J. P. Lee, L. M. Wells, B. Villa, *et al.*, "Controllable photonic time-bin qubits from a quantum dot," Phys. Rev. X **8**, 021078 (2018).
6. C. Liu, T.-X. Zhu, M.-X. Su, *et al.*, "On-demand quantum storage of photonic qubits in an on-chip waveguide," Phys. Rev. Lett. **125**(26), 260504 (2020).
7. J. M. Donohue, M. Agnew, J. Lavoie, *et al.*, "Coherent ultrafast measurement of time-bin encoded photons," Phys. Rev. Lett. **111**(15), 153602 (2013).
8. F. Bouchard, D. England, P. J. Bustard, *et al.*, "Quantum communication with ultrafast time-bin qubits," PRX Quantum **3**(1), 010332 (2022).

Optics EXPRESS

9. F. Bouchard, K. Bonsma-Fisher, K. Heshami, *et al.*, "Measuring ultrafast time-bin qudits," Phys. Rev. A **107**(2), 022618 (2023).
10. F. Bouchard, K. Fenwick, K. Bonsma-Fisher, *et al.*, "Programmable photonic quantum circuits with ultrafast time-bin encoding," Phys. Rev. Lett. **133**(9), 090601 (2024).
11. K. L. Fenwick, F. Bouchard, G. S. Thekkadath, *et al.*, "Photonic quantum walk with ultrafast time-bin encoding," Optica **11**(7), 1017–1023 (2024).
12. M. Yabuno, T. Takumi, F. China, *et al.*, "Ultrafast measurement of a single-photon wave packet using an optical kerr gate," Opt. Express **30**(4), 4999–5007 (2022).
13. N. Matsuda, R. Shimizu, Y. Mitsumori, *et al.*, "Observation of optical-fibre kerr nonlinearity at the single-photon level," Nat. Photonics **3**(2), 95–98 (2009).
14. A.-H. Fattah, A. M. Flatae, A. Farrag, *et al.*, "Ultrafast single-photon detection at high repetition rates based on optical kerr gates under focusing," Opt. Lett. **46**(3), 560–563 (2021).
15. J. E. Midwinter and J. Warner, "Up-conversion of near infrared to visible radiation in lithium-meta-niobate," J. Appl. Phys. **38**(2), 519–523 (1967).
16. W.-H. Jiang, J.-H. Liu, Y. Liu, *et al.*, "1.25 ghz sine wave gating ingaas/inp single-photon detector with a monolithically integrated readout circuit," Opt. Lett. **42**(24), 5090–5093 (2017).
17. A. P. VanDevender and P. G. Kwiat, "High-efficiency single photon detection via frequency up-conversion," in *Quantum Information and Computation*, vol. 5105 E. Donkor, A. R. Pirich, and H. E. Brandt, eds., International Society for Optics and Photonics (SPIE, 2003), pp. 216–224.
18. M. A. Albota and F. N. C. Wong, "Efficient single-photon counting at 1.55 μm by means of frequency upconversion," Opt. Lett. **29**(13), 1449–1451 (2004).
19. N. Yao, Q. Yao, X.-P. Xie, *et al.*, "Optimizing up-conversion single-photon detectors for quantum key distribution," Opt. Express **28**(17), 25123–25133 (2020).
20. J.-P. W. MacLean, J. M. Donohue, and K. J. Resch, "Direct characterization of ultrafast energy-time entangled photon pairs," Phys. Rev. Lett. **120**(5), 053601 (2018).
21. R.-B. Jin, T. Saito, and R. Shimizu, "Time-frequency duality of biphotons for quantum optical synthesis," Phys. Rev. Appl. **10**(3), 034011 (2018).
22. R. Jin, K. Tazawa, N. Asamura, *et al.*, "Quantum optical synthesis in 2d time-frequency space," APL Photonics **6**(8), 086104 (2021).
23. N. Namekata, N. Kobayashi, K. Nomura, *et al.*, "Quantum optical tomography based on time-resolved and mode-selective single-photon detection by femtosecond up-conversion," Sci. Rep. **13**(1), 21080 (2023).
24. P. Koviri, H. Komori, H. Tian, *et al.*, "Single-photon level ultrafast time-resolved measurement using two-color dual-comb-based asynchronous linear optical sampling," Appl. Phys. Express **17**(2), 022001 (2024).
25. O. Kuzucu, F. N. C. Wong, S. Kurimura, *et al.*, "Time-resolved single-photon detection by femtosecond upconversion," Opt. Lett. **33**(19), 2257–2259 (2008).
26. O. Kuzucu, F. N. C. Wong, S. Kurimura, *et al.*, "Joint temporal density measurements for two-photon state characterization," Phys. Rev. Lett. **101**(15), 153602 (2008).
27. M. Allgaier, G. Vigh, V. Ansari, *et al.*, "Fast time-domain measurements on telecom single photons," Quantum Sci. Technol. **2**(3), 034012 (2017).
28. M. Allgaier, V. Ansari, L. Sansoni, *et al.*, "Highly efficient frequency conversion with bandwidth compression of quantum light," Nat. Commun. **8**(1), 14288 (2017).
29. N. E. Yu, S. Kurimura, Y. Nomuta, *et al.*, "Stable high-power green light generation with thermally conductive periodically poled stoichiometric lithium tantalate," Jpn. J. Appl. Phys. **43**(No. 10A), L1265–L1267 (2004).
30. J. Hirohashi, T. Tago, O. Nakamura, *et al.*, "Characterization of GRIIRA properties in $LiNbO_3$ and $LiTaO_3$ with different compositions and doping," in *Nonlinear Frequency Generation and Conversion: Materials, Devices, and Applications VII*, vol. 6875 P. E. Powers, ed., International Society for Optics and Photonics (SPIE, 2008), p. 687516.
31. S. V. Tovstonog, S. Kurimura, I. Suzuki, *et al.*, "Thermal effects in high-power CW second harmonic generation in Mg-doped stoichiometric lithium tantalate," Opt. Express **16**(15), 11294–11299 (2008).
32. S. Kase and K. Ohi, "Optical absorption and interband Faraday rotation in $LiTaO_3$ and $LiNbO_3$," Ferroelectrics **8**(1), 419–420 (1974).
33. N. A. Chaitanya, A. Aadhi, M. V. Jabir, *et al.*, "High-power, high-repetition-rate, yb-fiber laser based femtosecond source at 355 nm," Opt. Lett. **40**(18), 4269–4272 (2015).
34. G. D. Boyd and D. A. Kleinman, "Parametric interaction of focused gaussian light beams," J. Appl. Phys. **39**(8), 3597–3639 (1968).
35. H. H. Lim, S. Kurimura, T. Katagai, *et al.*, "Temperature-dependent sellmeier equation for refractive index of 1.0 mol% Mg-doped stoichiometric lithium tantalate," Jpn. J. Appl. Phys. **52**(3R), 032601 (2013).
36. H. Kamada, M. Asobe, T. Honjo, *et al.*, "Efficient and low-noise single-photon detection in 1550 nm communication band by frequency upconversion in periodically poled $LiNbO_3$ waveguides," Opt. Lett. **33**(7), 639–641 (2008).
37. G.-L. Shentu, J. S. Pelc, X.-D. Wang, *et al.*, "Ultralow noise up-conversion detector and spectrometer for the telecom band," Opt. Express **21**(12), 13986–13991 (2013).
38. L. Y. Liang, J. S. Liang, Q. Yao, *et al.*, "Compact all-fiber polarization-independent up-conversion single-photon detector," Opt. Commun. **441**, 185–189 (2019).

Optics EXPRESS

39. K. Zhang, J. He, and J. Wang, "Two-way single-photon-level frequency conversion between 852 nm and 1560 nm for connecting cesium D2 line with the telecom C-band," Opt. Express **28**(19), 27785–27796 (2020).
40. N. E. Yu, J. H. Ro, and M. Cha, "Broadband quasi-phase-matched second-harmonic generation in MgO-doped periodically poled $LiNbO_3$ at the communications band," Opt. Lett. **27**(12), 1046–1048 (2002).
41. N. E. Yu, S. Kurimura, K. Kitamura, *et al.*, "Efficient frequency doubling of a femtosecond pulse with simultaneous group-velocity matching and quasi phase matching in periodically poled, MgO-doped lithium niobate," Appl. Phys. Lett. **82**(20), 3388–3390 (2003).
42. D. Shayovitz, H. Herrmann, W. Sohler, *et al.*, "Real-time coherent detection of phase modulated ultrashort pulses after time-to-space conversion and spatial demultiplexing," Opt. Express **22**(25), 31138–31145 (2014).
43. R. Tamaki, M. Suzuki, S. Kusaba, *et al.*, "Ultrafast pump-probe spectroscopy via chirped-pulse up-conversion with dispersion compensation," Opt. Express **31**(24), 40142–40150 (2023).
44. Y. Kochi, Y. Kinoshita, S. Kurimura, *et al.*, "Femtosecond time-bin pulse transfer and retrieval on photon-echo-based quantum memory using quantum dots," in *Quantum Sensing and Nano Electronics and Photonics XIX*, vol. 12430 M. Razeghi, G. A. Khodaparast, and M. S. Vitiello, eds., International Society for Optics and Photonics (SPIE, 2023), p. 1243014.
45. Y. Kochi, Y. Kinoshita, S. Kurimura, *et al.*, "Improved efficiency of generating femtosecond photon echoes from quantum dots using chirped pulses and time resolved measurement by frequency up-conversion technique," in *Ultrafast Phenomena and Nanophotonics XXVIII*, vol. 12884 M. Betz and A. Y. Elezzabi, eds., International Society for Optics and Photonics (SPIE, 2024), p. 128840E.

144.213.253.16 (ts 2024-12-25 05:11:32)